

Journal of Biomedical Optics

SPIEDigitalLibrary.org/jbo

Deep optical imaging of tissue using the second and third near-infrared spectral windows

Laura A. Sordillo
Yang Pu
Sebastião Pratavieira
Yury Budansky
Robert R. Alfano

Deep optical imaging of tissue using the second and third near-infrared spectral windows

Laura A. Sordillo,^a Yang Pu,^a Sebastião Pratavieira,^{a,b} Yury Budansky,^a and Robert R. Alfano^{a,*}

^aCity College of the City University of New York, Institute for Ultrafast Spectroscopy and Lasers, and Department of Physics, 160 Convent Avenue, New York 10031

^bUniversidade de São Paulo, Instituto de Física de São Carlos, São Carlos 05508-060, Brasil

Abstract. Light at wavelengths in the near-infrared (NIR) region allows for deep penetration and minimal absorption through high scattering tissue media. NIR light has been conventionally used through the first NIR optical tissue window with wavelengths from 650 to 950 nm. Longer NIR wavelengths had been overlooked due to major water absorption peaks and a lack of NIR-CCD detectors. The second NIR spectral window from 1100 to 1350 nm and a new spectral window from 1600 to 1870 nm, known as the third NIR optical window, were investigated. Optical attenuation measurements from thin tissue slices of normal and malignant breast and prostate tissues, pig brain, and chicken tissue were obtained in the spectral range from 400 to 2500 nm. Optical images of chicken tissue overlying three black wires were also obtained using the second and third spectral windows. Due to a reduction in scattering and minimal absorption, longer attenuation lengths and clearer optical images could be seen in the second and third NIR optical windows compared to the conventional first NIR optical window. A possible fourth optical window centered at 2200 nm was noted. © 2014 Society of Photo-Optical Instrumentation Engineers (SPIE) [DOI: 10.1117/1.JBO.19.5.056004]

Keywords: near-infrared light; scattering; turbid media; near-infrared imaging; imaging through turbid media; near-infrared therapeutic window; second and third optical windows; breast cancer; attenuation length; optical mammography.

Paper 140143R received Mar. 4, 2014; revised manuscript received Apr. 9, 2014; accepted for publication Apr. 10, 2014; published online May 7, 2014.

1 Introduction

It is well known that light at wavelengths in the visible to near-infrared (NIR) range from 650 to 1350 nm is a noninvasive optical tool to detect and image tissue abnormalities. Optical mammography, for example, has been studied as an alternative NIR technique, which utilizes NIR light to image cancerous breast lesions. NIR light allows for greater depth penetration, minimal absorption, and scattering into tissue than does shorter wavelengths in the visible region. By choosing the appropriate wavelength of light and charge-coupled device (CCD) detector, one can increase the penetration depth into tissue media and produce clearer optical images. In 1929, Max Cutler reported using white light and optical transillumination to image the breast.¹ He had hoped to replace the use of x-rays with the use of longer wavelengths of light in the visible and NIR regions; however, due to lack of appropriate detectors and laser sources, he was unsuccessful. Since that time, better detectors, laser sources, and computer technologies have allowed others, such as Chance and Alfano, to use frequency modulation and time-resolved imaging, respectively, to image tissue abnormalities.^{2,3} Nowadays, the NIR region with wavelengths from 650 to 950 nm, called the first therapeutic window, is conventionally used for most NIR tissue imaging studies and photodynamic therapy applications.⁴⁻⁸ Due to Rayleigh scattering, (which varies as the inverse fourth power of the wavelength) and due to Mie scattering (which varies as $1/\lambda^n$ with $n \geq 1$) at longer wavelengths, there is less scattering and minimal absorption when using this window (longer wavelengths) than there is in the visible

range (shorter wavelengths). For these reasons, it is expected that the longer NIR wavelengths of light, above 950 nm, would show less scattering and higher contrast images than the first optical window.

The use of longer NIR wavelengths for tissue studies, at the second (1100 to 1350 nm) and third (1600 to 1870 nm) NIR optical windows, is introduced and investigated in this paper. Optical attenuation from normal and malignant breast and prostate tissues, pig brain, and chicken tissue in the spectral range of 400 to 2500 nm was measured. With these NIR optical windows and an InGaAs camera detector, optical images of chicken tissue overlying black wires were also obtained. The most effective measure in the reduction of mortality and morbidity from cancer and other disease conditions is detection at an early stage of disease by x-ray mammography.⁹ The use of these longer NIR wavelengths with new two dimensional (2-D) photodetectors and high-speed computers may allow for improved methods of imaging breast and other tissues.

1.1 Imaging through Tissue Media

Light through turbid media can be described by the trajectories (diffusive, ballistic, and snake) of photons.¹⁰ With increasing propagation distance, these photons will be attenuated by the effects of scattering and absorption, resulting in a reduction in image quality. Absorption of light in tissue media can occur by selected biomolecules, such as collagen and elastin, lipids, hemoglobin or water in tissue media, while scattering can be caused by cells or intracellular matrix. Water molecules, in particular, greatly affect image quality and penetration depth

*Address all correspondence to: Robert R. Alfano, E-mail: alfano@sci.cuny.edu

due to strong absorption peaks from vibrational modes at ~ 900 , ~ 1200 , ~ 1400 and ~ 1900 nm. These effects can be minimized by imaging through thin tissue slices (less than 1 mm), thus allowing the ballistic photons (described by Lambert–Beer’s intensity law) to govern over the diffusive photons. These photons can be measured by the total attenuation coefficient (μ_t), where μ_t is the inverse of the total length traveled by the ballistic photons in the tissue media [also known as the total attenuation length (l_t)] and is determined by combining the absorption (μ_a) and scattering (μ_s) coefficients ($\mu_t = \mu_a + \mu_s$).^{11–13}

1.2 First, Second, and Third Optical Windows

In the first region of minimal water absorption between water peak maxima (first NIR optical window from 650 to 950 nm), image quality is reduced due to strong absorption peaks from lipids and from hemoglobin and deoxyhemoglobin, and is blurred due to the molecular process of Rayleigh/Mie scattering. Figure 1 highlights the absorption properties of deoxyhemoglobin (Hb), hemoglobin (HbO₂), and water (H₂O) in the first optical window.¹⁴

Recently, a new NIR wavelength transmission window from 1100 to 1350 nm, located between two additional water peaks, has been used for *in vivo* imaging.¹⁵ Limited studies on this second optical window have been done due to strong water absorption and lack of 2-D NIR photodetectors. Today, advances in the spectral response of NIR-CCD image sensors have made NIR camera specificity possible up to a wavelength of 2200 nm. As a result, longer wavelengths can be used. We report on the use of a new third NIR spectral region from 1600 to 1870 nm, between two strong water peaks (1444 and 1950 nm), to image deeply into tissue media.^{16,17} This region had been previously ignored due to water absorption. However, Yoo and Alfano have demonstrated that a small amount of absorption can help to minimize the detection of diffusive photons, which cause images to blur, and can highlight the ballistic and snake photons, which are responsible for producing clearer images.¹⁸

2 Experimental

Optical attenuation measurements from tissue in the second and third NIR spectral windows (1100 to 1350 nm and 1600 to 1870 nm, respectively) were obtained and compared with those from the first NIR spectral window. Optical attenuation measurements using a possible fourth optical window were

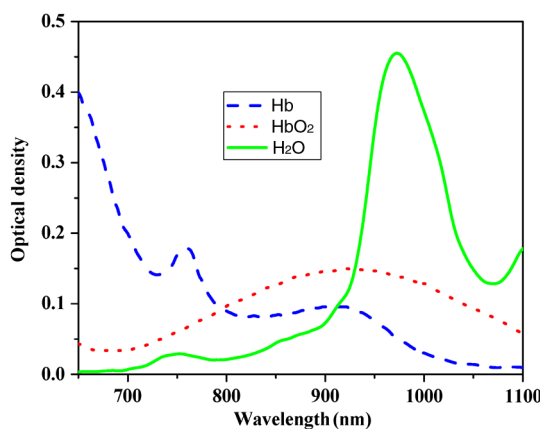


Fig. 1 Absorption spectra of deoxyhemoglobin (Hb), hemoglobin (HbO₂), and water in the visible and NIR regions.

obtained but not explored due to lack of detector imaging sensitivity. Normal and malignant human breast and prostate tissues were supplied by the national disease research interchange and the cooperative human tissue network under an institutional review board protocol. Breast cancer tissues were obtained from two patients. Patient (1) was a 48-year-old woman with lobular carcinoma, which was estrogen receptor positive, progesterone receptor positive, and Her-2-Neu positive. Patient (2) was a 51-year-old woman with ductal carcinoma, which was estrogen receptor positive, progesterone receptor positive, and Her-2-Neu negative. The tissue samples were not fixed or chemically treated. Samples were kept in a low-temperature freezer (minus 80°C) to preserve freshness. Fresh chicken muscle from the breast region for optical imaging studies was also acquired and placed in a conventional freezer $\sim 18^\circ\text{C}$ (0°F). Once frozen, the chicken tissue was cut into thin slices of various thicknesses. Prior to the spectroscopic studies, all tissue samples were removed from the freezer and allowed to reach room temperature. The pig brain sample was not frozen prior to the study; measurements were performed within 24 h of resection.

2.1 Optical Attenuation

The optical density spectra from tissue slices were obtained using the Varian Cary 500 Scan UV/VIS/NIR spectrophotometer in the spectral range of 400 to 2500 nm. Thin tissue slices were necessary for the ballistic light to dominate over the diffusive light. Optical attenuation measurements from normal and malignant human breast and prostate tissues, pig brain, and chicken tissue were obtained at each of the four optical windows. Breast and prostate tissue samples were cut into thicknesses of ~ 50 , 100, and 200 μm and placed in thin quartz cuvettes. Pig brain tissue was cut into a thickness of ~ 100 μm . The chicken tissue samples were acquired from two regions: the muscle and the fatty outermost regions.

2.2 Imaging Using the Second and Third Optical Windows

Transmission images (322×240 pixels) of chicken breast tissue with black wires of various thicknesses were obtained using the second and third NIR optical windows and the optical setup in Fig. 2. Three wires with thicknesses of 0.75, 0.95, and 1.35 mm were inserted between a chicken tissue layer of 1.6 mm (located near the front of the light source) and thin chicken slices of various thicknesses (located near the front of the detector). The chicken tissue slices were measured at thicknesses of 1.6, 2.8, 3.9, and 7.4 mm.

The optical setup (seen in Fig. 2) includes a halogen lamp light source with spectral distribution from 200 to 2500 nm, selective filters at 1120 nm HW 40 and at 1500 nm longpass for the second and third optical windows, respectively, and an IR-CCD InGaAs camera (Goodrich Sensors Inc. high response camera SU320KTSW-1.7RT, Princeton, New Jersey) with spectral response between 0.9 and 1.7 μm (highlighting the second and third optical windows). The 1500 nm longpass filter was used to cutoff light of wavelengths below 1500 nm. This allowed for the transmission of light from the third window with wavelengths from 1600 to 1700 nm.

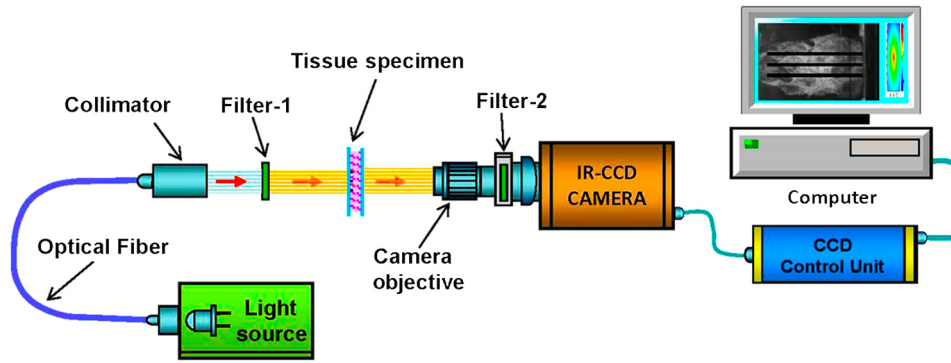


Fig. 2 Setup for optical imaging of tissue specimen using the second and third optical windows.

3 Results and Discussion

3.1 Optical Attenuation Spectra of Human Prostate Tissue, Human Breast Tissue, and Pig Brain

Figure 3 shows the spectrum of total attenuation coefficient (μ_t) in (mm^{-1}) from thin prostate tissue with a thickness of $200 \mu\text{m}$ in the spectral range of 400 to 2500 nm with four optical windows highlighted. The total attenuation coefficient (μ_t) is defined by combining the absorption (μ_a) and scattering (μ_s) coefficients where ($\mu_a + \mu_s$) equals μ_t . The ballistic light in the thin tissue media depends on μ_a plus μ_s .^{19–20} The total attenuation coefficient (μ_t) was calculated using Eq. (1)

$$\mu_t = \frac{(2.303 \times \text{OD})}{z}, \quad (1)$$

where OD corresponds to the optical density results from the tissue and z is the thickness of the tissue sample. Equation (1) was derived from the light intensity I over the incident light I_0 and is described by the Lambert–Beer's Eq. (2)

$$\frac{I}{I_0} = \exp[-(\mu_t z)] = 10^{-\text{OD}}. \quad (2)$$

The normal prostate tissue sample used to acquire the spectrum in Fig. 3 was cut into additional thicknesses of 50 and $100 \mu\text{m}$. Figure 4 shows the corresponding spectra of the

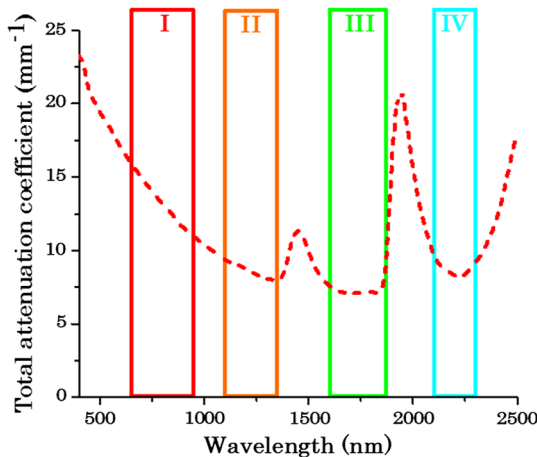


Fig. 3 Spectrum of the total attenuation coefficient (μ_t) from normal prostate tissue using the I, II, III, and a possible IV optical windows.

total attenuation lengths (l_t) in micrometers, in the spectral range of 400 to 2500 nm, from normal prostate tissues at thicknesses of 50, 100, and $200 \mu\text{m}$, where the total attenuation lengths (l_t) are the inverse of the total attenuation coefficient (μ_t) (seen in Fig. 3).

The total attenuation lengths (l_t) are noticeably larger in the third optical window with a peak maximum at 1835 nm.

Figures 5 and 6 show the total attenuation lengths (l_t) in micrometers from normal and malignant prostate and breast tissues with thicknesses of $200 \mu\text{m}$. A larger total attenuation length (l_t) occurs in the new third optical window compared to the first, second, and fourth optical windows. We also notice that l_t from normal tissue is larger compared to the malignant tissue samples.

Table 1 summarizes the results obtained from the total attenuation lengths (l_t) of normal and cancerous breast and prostate tissues, pig brain, and chicken tissue at selected wavelengths representing the four optical windows. The total attenuation lengths (l_t) were measured at wavelengths of 750, 1200, 1700, and 2200 nm. Wavelengths of 1200 and 1700 nm were chosen to correspond to wavelengths in the second and third optical windows, and were used in the optical imaging setup. As the wavelength is increased, μ_s is reduced and μ_a dominates. The maximum penetration depths (l_t) occurred in the third optical window around 1835 nm for all tissue samples. Normal prostate tissue with a thickness of $100 \mu\text{m}$ had a penetration depth of $\sim 800 \mu\text{m}$ at a wavelength of 1700 nm using the third optical

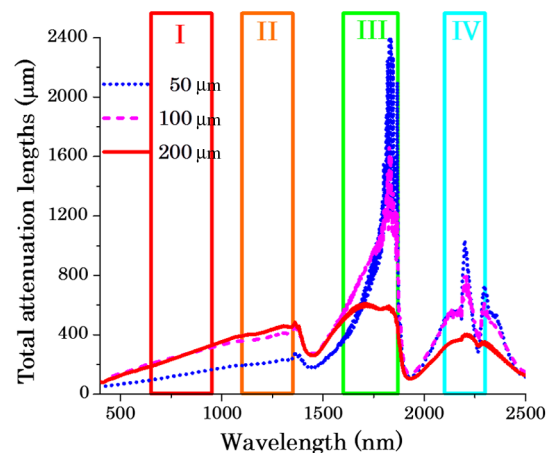


Fig. 4 Spectra of the total attenuation lengths (l_t) in μm from normal prostate tissue at different thicknesses of 50, 100 and $200 \mu\text{m}$ using the I, II, III, and IV optical windows.

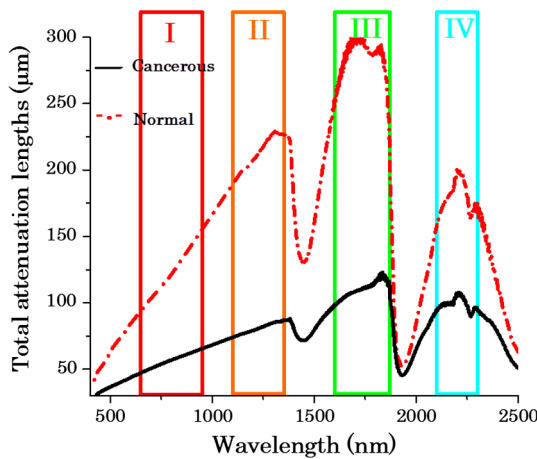


Fig. 5 Spectra of the total attenuation lengths (l_t) in μm from normal and cancerous prostate tissues using the I, II, III, and IV optical windows.

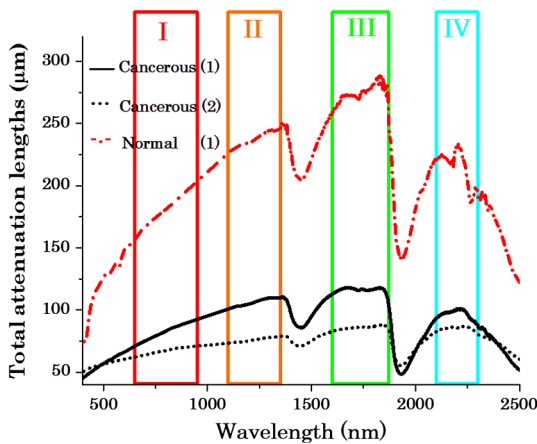


Fig. 6 Spectra of the total attenuation length (l_t) in μm from normal and cancerous breast tissues from two patients using the I, II, III, and IV optical windows.

window. Results from chicken tissue samples show a slight decrease from the second optical window to the third optical window. We suspect that this is due to the large amount of protein in the chicken samples compared to all the other tissue samples, which have a higher lipid content. At wavelengths greater than 1900 nm (in the fourth optical window), a reduction in l_t can be seen due to a combination of vibrational modes from lipids, collagen, and water molecules in the tissues. We also note that l_t is greater in the fourth optical window than the first optical window.

3.2 Images of Chicken Tissue and Wires at Different Depths

Transmission images, seen in Fig. 7 and acquired using the optical setup in Fig. 2, illustrate the appearance of the black wires [0.75 mm (left), 0.95 mm (middle) and 1.35 mm (right)] through tissue slices (ranging from no overlying tissue to a layer of 3.9 mm in thickness with a bottom layer of 1.8 mm). Light from wavelengths in the second and third windows was able to penetrate the thick tissue layer and give clear images of the hidden wires. The images of the three wires, using the second

Table 1 Optical properties l_t (μm) from tissues in the four (I, II, III, IV) optical windows from wavelengths at 750, 1200, 1700, and 2200 nm.

Tissue details		Total attenuation lengths l_t (μm)			
Depth (μm)	Type	I	II	III	IV
50	Prostate normal	120	207	611	1038
100	Prostate normal	245	373	818	731
200	Prostate normal	207	414	589	401
100	Prostate cancer	161	168	206	209
200	Prostate cancer	101	159	217	213
50	Breast normal (1)	130	174	250	270
100	Breast normal (1)	209	242	300	319
200	Breast normal (1)	167	234	271	232
100	Breast cancer (1)	169	311	438	365
200	Breast cancer (1)	66	75	86	86
50	Breast cancer (2)	23	30	33	33
100	Breast cancer (2)	66	99	127	132
200	Breast cancer (2)	79	105	117	101
100	Pig brain	190	235	279	291
200	Chicken muscle	90	125	120	94
200	Chicken fat	90	118	117	99

and third optical windows, and an overlying 7.4 mm thickness (not shown), were apparent on the screen during the experimental procedure and before the imaging process. Images of the three wires and chicken tissue were recorded with a transmission maximum penetration depth of 3.9 mm.

Penetration depth analysis was done on the images of the three (1, 2, and 3) wires through chicken breast tissue at the second and third optical windows. The corresponding digitized spatial intensity distributions of the images were obtained by integrating the image intensity over the horizontal rectangular region [as marked by the black boxes in Figs. 7(a)–7(d)]. Plots of intensity (arbitrary units) versus distance (pixels) of the wires and chicken breast tissue in the second and third windows were also obtained and are shown in Figs. 7(a)–7(d). The image intensity can be described by the light intensity transmitted through the chicken breast tissue onto the three wires.

Table 2 summarizes the contrast results from images of chicken tissue of different thicknesses and three wires using the second and third optical windows. The degree of contrast can be calculated as the intensity of signal minus intensity of background divided by intensity of signal plus intensity of background times 100. The second and third optical windows have similar signal to background ratios. From Figs. 7(a)–7(d) and Table 2, images from the second and third optical windows show minimal noise and demonstrate the three black wires through tissue media. Images of the three wires with an overlying tissue thickness of 1.6 mm have the highest contrast

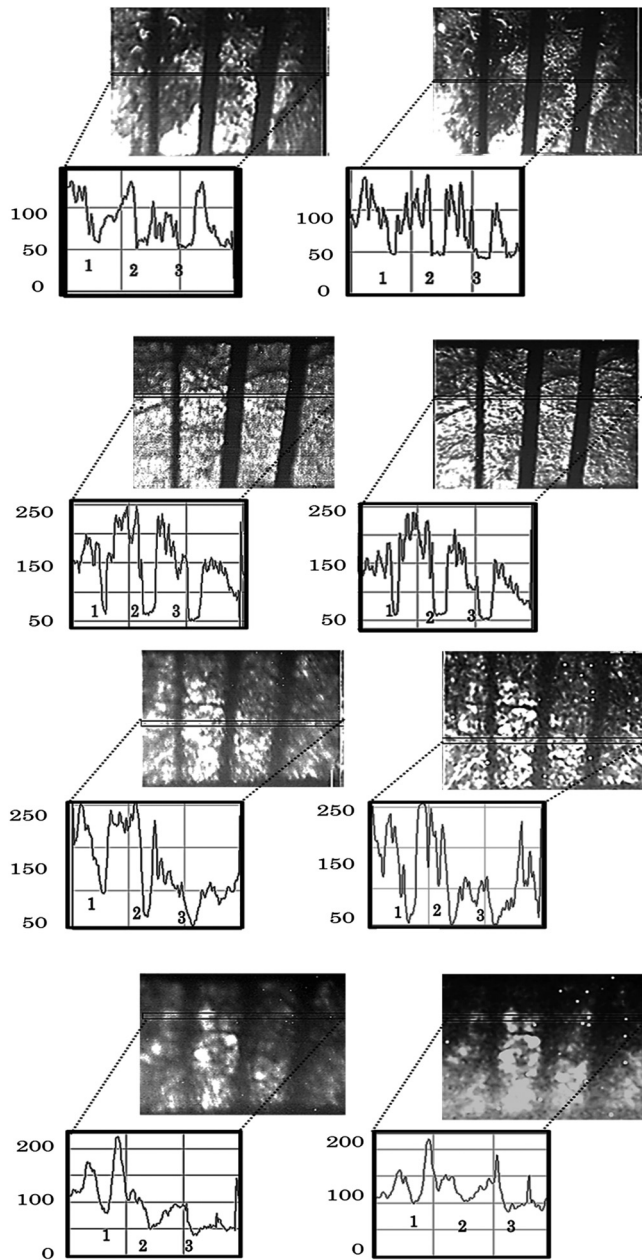


Fig. 7 Transmission images of chicken tissue with thicknesses (a) no overlying tissue, (b) 1.6 mm, (c) 2.8 mm, and (d) 3.9 mm covering three black wires of different depths with corresponding spatial intensity distribution spectra using the second (II) and third (III) optical windows.

Table 2 Contrast results from the images of the three wires and chicken breast tissue of various thicknesses.

Total thickness (mm)	Top thickness (mm)	Second window (%)	Third window (%)
1.8	0	67.8	76.4
3.4	1.6	75.2	76.2
4.6	2.8	58.5	43.1
5.7	3.9	32.1	24.0

percentage while the images of the wires with an overlying layer of 3.9 mm are slightly blurred but still visible. Due to greater muscle content in the chicken tissue at thicknesses of 2.8 and 3.9 mm, the second optical window has a greater percent contrast than the third optical window.

4 Conclusion

Due to a reduction in scattering in tissue media at longer NIR wavelengths, longer attenuation and clearer images can be seen in the second and third NIR optical windows and may provide additional information to that observed using the conventional first NIR window. Deeper NIR images can be achieved due to a reduction in the scattering coefficient, allowing the absorption coefficient to be the main determinant of image quality. Optimizing tissue image contrast from the NIR second and third optical windows is needed. Better NIR light sources, such as intense tunable lasers Forestrite (1150 to 1300 nm), Cunyite (1200 to 1500 nm) and LSO (1110 to 1600 nm), the supercontinuum laser source (400 to 2,400 nm), or semiconductor laser diodes, will eliminate photon starvation and improve sensitivity and signal to noise ratios.²¹ Using a more intense NIR light source in optical mammography could provide deeper depth penetration and better optical images of abnormalities, which are hidden behind normal tissue. We also note that this technique may be of benefit when imaging objects through fog or cloudy water.^{22,23}

Acknowledgments

This research is supported by U. S. Army Medical Research and Material Command USAMRMC Grant No. W81XWH-11-1-0335 (CUNY RF # 47204-00-01). We thank Lingyan Shi for slicing the tissue samples and Peter P. Sordillo MD, PhD for reviewing this paper.

References

1. M. Cutler, "Transillumination as an aid in the diagnosis of breast lesions," *Surg. Gynecol. Obstet.* **48**, 721–729 (1929).
2. B. Chance et al., "A novel method for fast imaging of brain function, non-invasively, with light," *Opt. Express* **2**(10), 411–423 (1998).
3. L. Wang, P. P. Ho, and R. R. Alfano, "Time-resolved Fourier spectrum and imaging in highly scattering media," *Appl. Opt.* **32**(26), 5043–5048 (1993).
4. R. R. Anderson and J. A. Parrish, "The optics of human skin," *J. Invest. Dermatol.* **77**(1), 13–19 (1981).
5. J. V. Frangioni, "In vivo imaging near-infrared fluorescence imaging," *Curr. Opin. Chem. Biol.* **7**(5), 626–634 (2003).
6. D.C. Sordillo et al., "A novel approach to Paget's disease diagnosis and monitoring using near-infrared absorption spectroscopy," *Proc. SPIE* **8565**, 856566 (2013).
7. J. A. Curcio and C. C. Petty, "The near infrared spectrum of liquid water," *J. Opt. Soc. Am.* **41**(5), 302–304, (1951).
8. L.A. Sordillo et al., "Time-resolved fluorescence for breast cancer detection using an octeotote-indocyanine green derivative dye conjugate," *Proc. SPIE* **8577**, 857708 (2013).
9. American Cancer Society (ACS) <http://www.cancer.org/>.
10. L. Wang et al., "Ballistic 2D imaging through scattering walls using an ultrafast optical Kerr Gate," *Science* **253**(5021), 767–771 (1991).
11. L. Yang and S. J. Miklavcic, "Theory of light propagation incorporating scattering and absorption in turbid media," *Opt. Lett.* **30**(7), 792–794 (2005).
12. R. Weissleder, "A clearer vision for in vivo imaging," *Nat. Biotechnol.* **19**, 316–317 (2001).
13. J. Rao, A. Dragulescu-Andrasi, and H. Yao, "Fluorescence imaging in vivo: recent advances," *Curr. Opin. Biotechnol.* **18**(1), 17–25 (2007).

14. Y. Pu et al., "Two-photon excitation microscopy using the second singlet state of fluorescent agents within the tissue optical window," *J. Appl. Phys.* **114**(15), 153102 (2013).
15. A. M. Smith, M. C. Mancini, and S. Nie, "Bioimaging: second window for in vivo imaging," *Nat. Nanotechnol.* **4**, 710–711 (2009).
16. L.A. Sordillo et al., "Deep tissue imaging of microfracture and non-displaced fracture of bone using the second and third near-infrared therapeutic windows," *Proc. SPIE* **8926**, 89263V (2014).
17. L.A. Sordillo et al., "Third therapeutic spectral window for deep tissue imaging," *Proc. SPIE* **8940**, 89400V (2014).
18. K. M. Yoo, F. Liu, and R. R. Alfano, "Imaging through a scattering wall using absorption," *Opt. Lett.* **16**(14), 1068–1070 (1991).
19. K. M. Yoo and R. R. Alfano, "Time-resolved coherent and incoherent components of forward light scattering in random media," *Opt. Lett.* **15**(6), 320–322 (1990).
20. M. Kempe et al., "Ballistic and diffuse light detection in confocal and heterodyne imaging systems," *J. Opt. Soc. Am. A* **14**(1), 216–223 (1997).
21. R. R. Alfano, *The Supercontinuum Light Source*, Springer, New York (2006).
22. X. Ni and R. R. Alfano, "Free-space ballistic laser propagation of a pulse coded data stream through fog," *Appl. Opt.* **42**(35), 6980–6983 (2003).
23. K. M. Yoo, Q. Xing, and R. R. Alfano, "Imaging objects hidden in highly scattering media using femtosecond second-harmonic-generation cross-correlation time gating," *Opt. Lett.* **16**(13), 1019–1021 (1991).

Laura A. Sordillo, MS is a researcher at the Institute for Ultrafast Spectroscopy and Lasers in the physics department at The City College of CUNY. She has developed a novel portal device for assessment of cancerous lesions, studied the use of an octreotate-indocyanine dye to target breast cancer, and investigated the use of NIR light to image microfractures of human tibial bone. She is recipient of the CCNY-MSKCC Partnership graduate award.

Yang Pu, PhD, is an imaging specialist at the University of California at Irvine. He is a multidisciplinary researcher in the fields of biomedical optics and radiology. His research is concentrated on breaking two limits of optics: 1. Enhancing the resolution of microscope to break the limitation of diffraction; and 2. Imaging deep organ of large animal and human using optical technique.

Robert R. Alfano is a distinguished professor of Science and Engineering at The City College of CUNY. He has pioneered many applications of light and photonics technologies to the study of biological, biomedical and condensed matter systems, invented and used in his research supercontinuum and novel tunable solid state lasers. He has received his PhD in physics from New York University and is a Fellow of American Physical Society, Optical Society of America, and IEEE.

Biographies of the other authors are not available.